Nonlinear Effects in T-Branch Junctions

Javier Mateos, Beatriz G. Vasallo, Daniel Pardo, Tomás González, Emmanuelle Pichonat, Jean-Sébastien Galloo, Sylvain Bollaert, Yannick Roelens, and Alain Cappy, *Senior Member, IEEE*

***Abstract*—The negative potential appearing at the central branch of T-branch junctions (TBJs) when biasing left and right contacts in push-pull fashion has been found to appear under high biasing not only for short (ballistic) TBJs but also for long (diffusive) ones. By means of a microscopic Monte Carlo simulation we are able to explain this nonlinear effect as a consequence of intervalley scattering mechanisms leading to the emergence of an accumulation domain that modifies the electronic potential profile within the devices.**

***Index Terms*—Ballistic devices, Monte Carlo (MC) simulation, three-terminal ballistic junctions.**

I. Introduction

BALLISTIC TRANSPORT appears when the size of electronic devices is reduced below the electron mean-free path. By using high mobility materials, current lithographic techniques allow the fabrication of nanometer-scale devices showing ballistic (or quasi-ballistic) transport even at room temperature. In these devices, some interesting nonlinear effects related to ballistic transport has been observed, for example, ballistic rectification [1], [2]. In this letter, we will focus on a ballistic effect predicted theoretically by Xu [3] and later measured in T-branch junctions (TBJs) [4]: the appearance of a negative potential at the central branch, V_C, when biasing in push-pull fashion the left and right branches (in contrast with the zero potential expected for diffusive structures). In order to better understand this effect we have fabricated TBJs with different lengths, and we have obtained negative values for V_C not only in the short/ballistic TBJs (already explained in [5] and [6]) but also in the long/diffusive ones. In this letter, by using our Monte Carlo (MC) model, the experimental results will be reproduced and a microscopic explanation for this nonlinear effect will be given.

II. Fabrication and Experimental Measurements

The layer structure used for the fabrication of the TBJs was grown by molecular-beam epitaxy on InP substrate.

Manuscript received December 15, 2003; revised February 9, 2004. This work was supported in part by the European Commission through the NANOTERA Project IST-2001-32517, by the Dirección General de Investigación (Ministerio de Ciencia y Tecnología) and FEDER through Project TIC2001-1754, by the Consejería de Cultura de la Junta de Castilla y León through Project SA057/02, and by the Institut de Recherche en Composants pour l'Information et la Communication Avancée (IRCICA).

J. Mateos, B. G. Vasallo, D. Pardo, and T. González are with the Departamento de Física Aplicada, Universidad de Salamanca, Salamanca, Spain (e-mail: javierm@usal.es). The review of this letter was arranged by Editor T. Mizutani.

E. Pichonat, J.-S. Galloo, S. Bollaert, Y. Roelens, and A. Cappy are with the Département Hyperfréquences et Semiconducteurs, Institut d'Electronique de Microélectronique et de Nanotechnologie U.M.R. C.N.R.S., Villeneuve D'Ascq Cédex, France.

Digital Object Identifier 10.1109/LED.2004.826571

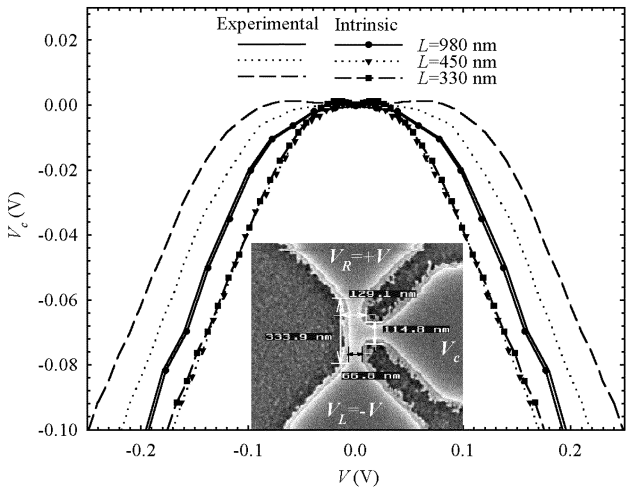

Fig. 1. V_C as a function of V for the TBJs with lengths of 980, 450, and 330 nm when biasing left and right branches in push-pull fashion, $V = V_L = -V_R$. The intrinsic results have been obtained considering a value for the access resistance of 2.5 kΩ. SEM image of the TBJs with $L = 330$ nm is shown as an inset.

It has a 15-nm-thick $In_{0.7}Ga_{0.3}As$ strained channel, with two $Al_{0.48}In_{0.52}As$ barriers and a δ-doped layer with $\delta = 4 \times 10^{12}$ cm^{-2}. Hall measurements of the wafer provides a mobility of 10 500 cm^2/Vs and a sheet electron density of 5.2×10^{12} cm^{-2} at room temperature. The geometry of the TBJs was defined by a high resolution negative e-beam resist Hydrogen SilsesQuioxane, exposed by a LEICA EBPG5000+ machine and a high diluted $H_3PO_4/H_2O_2/H_2O$ wet etching. Then Ni–Ge–Au–Ni–Au metals were evaporated and annealed to form ohmic contacts and, finally, Ti–Au bonding pads were realized. Fig. 1 shows the measured V_C in the fabricated TBJs with lengths L of 980, 450, and 330 nm [the scanning electron microscope (SEM) image of the smallest one is shown as an inset]. The width of the branches W is around 65 nm. The values shown in Fig. 1, corresponding to V_C (V) under push-pull bias ($V_R = -V_L = V$), have been extracted from the raw push-fix electrical measurement ($V_R = 2 \times V$; $V_L = 0$). The typical parabolic-like $V_C(V)$ behavior is observed for the three devices in Fig. 1. It must be pointed out that some of the measurements showed a considerable asymmetry due to differences between the access resistances or a shift in the position of the central branch [6]. The experimental results shown here have been adjusted by averaging over positive and negative applied bias so that to make them symmetric.

For an understanding of the intrinsic performance of the TBJs, the effect associated to the resistance of the access paths and the contacts must be removed from the experimental data. For the calculation of the results of Fig. 1, we have considered

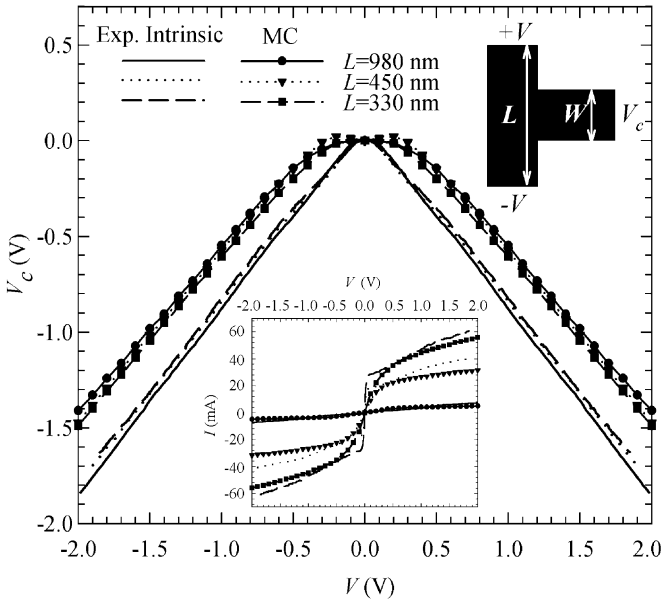

Fig. 2. V_C as a function of the intrinsic applied voltage when biasing in push-pull fashion $V = V_L = -V_R$ the TBJs of Fig. 1. The results obtained from the MC simulation of TBJs with the same geometries are also shown (lines with symbols). The insets show the *I–V* curves and the geometry of the simulated TBJs.

a resistance in each contact of $R_c = 2.5\ \mathrm{k}\Omega$, value extracted from the measurements of the resistance of channels with $W = 65$ nm and different lengths. In Fig. 1 it can be observed that R_c modifies considerably the $V_C(V)$ curve for the short TBJs, thus, showing an increase of the curvature of the intrinsic $V_C(V)$ for the shorter the TBJ (opposite behavior to that found in the extrinsic measurements). In Fig. 2 we can observe that as the length of the TBJs is increased the current decreases (inset of Fig. 2), but the $V_C(V)$ curves remain practically unchanged for high bias, showing negative values with a nearly constant unity slope ($|dV_C/dV| \approx 1$) for $V > 0.2$ V. The negative values for V_C shown in Fig. 1 are known to appear for low bias due to ballistic electron transport [3]–[6], but they also appear for the long structures, when transport is diffusive (or at least, quasidiffusive, since for the 1-μm-long TBJ MC simulations show that electrons overcome more than 20 scattering events during the transit time between left and right contacts). In that case, it is expected that the horizontal branch of the TBJ behaves as a classic resistance, with a linear *I–V* curve, and so the potential at the center should be 0. On the contrary, some different nonlinear effect takes place when strongly biasing long TBJs.

III. Monte Carlo Simulations

In Fig. 2 we have also represented the results of the MC simulation of the TBJs with the geometries shown before ($L = 980$, 450, and 330 nm and $W = 65$ nm). The access regions were not simulated, so that the simulation domain includes only the intrinsic part of the TBJs, sketched in the inset of Fig. 2. The two-dimensional top-view simulations were performed by considering a background doping $N_{Db} = 10^{17}\ \mathrm{cm}^{-3}$ (to account for the fixed charge in the different layers, but with no impurity scattering [5], [6]), injecting contacts with $N_c = 4 \times 10^{17}\ \mathrm{cm}^{-3}$

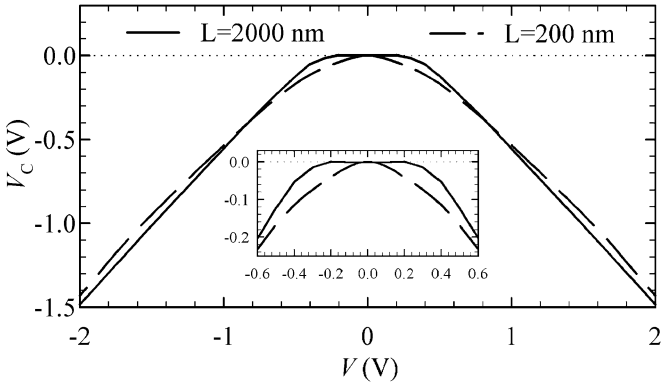

Fig. 3. V_C as a function of the applied voltage V when biasing in push-pull fashion $V = V_L = -V_R$ left and right branches of TBJs with different lengths: one ballistic ($L = 200$ nm, dashed line) and one diffusive ($L = 2000$ nm, solid line). A magnification of the low-bias region is shown as an inset.

and a surface charge density $\sigma = 0.3 \times 10^{12}\ \mathrm{cm}^{-3}$ (to take into account the lateral surface potential). With these parameters, a good overall agreement with the intrinsic experimental results is found.

In previous works [6], [7], our MC model has already been used to successfully explain the ballistic effects appearing in various nanometer scale devices, but no attention was paid to hot-electron effects appearing when the applied voltage is increased. In Figs. 1 and 2, one can clearly observe that when the bias is sufficiently increased V_C shows negative values not only for the short/ballistic TBJs, but also for the long ones. To explain this fact, we have performed MC simulations of two extreme cases of TBJs: one short/ballistic ($L = 200$ nm) and one long/diffusive ($L = 2\ \mu$m). Fig. 3 shows the values of V_C in both devices obtained with the MC simulation. A good agreement is found with the intrinsic results of Fig. 1: V_C is null in the diffusive TBJ for $V < 0.2$ V (as expected within its ohmic regime), while the short one shows the well known ballistic-related bell-shape. Only in this region of low-biasing the ballistic/diffusive character of transport inside the TBJs can be discriminated from these measurements, since, as observed in Figs. 2 and 3, for high V both short and long devices show negative V_C.

In order to understand the microscopic processes leading to the previous results, in Fig. 4 the horizontal profiles of concentration and potential in the long TBJ are plotted as a function of the x position for different bias conditions. For low V the concentration is almost constant within the whole TBJ [Fig. 4(a)] so that the potential drop is the same at both sides of the TBJ. As a consequence, as long as the TBJ remains in the ohmic region ($V < 0.2$ V) the potential measured at the central branch is nearly 0. On the other hand, in the short TBJ the electron concentration shows a strong asymmetry even for low applied voltages [inset of Fig. 4(a)], thus providing the characteristic negative values for V_C [5], [6]. When increasing the bias, the progressive electron heating leads to the onset of intervalley transfer. Consequently, electrons increase their effective mass and an accumulation domain appears near the anode [Fig. 4(a)]. As seen in Fig. 4(b), when this domain grows, the shape of the electric potential is strongly changed, and the potential drop concentrates in the most resistive part of the TBJ (the near-anode

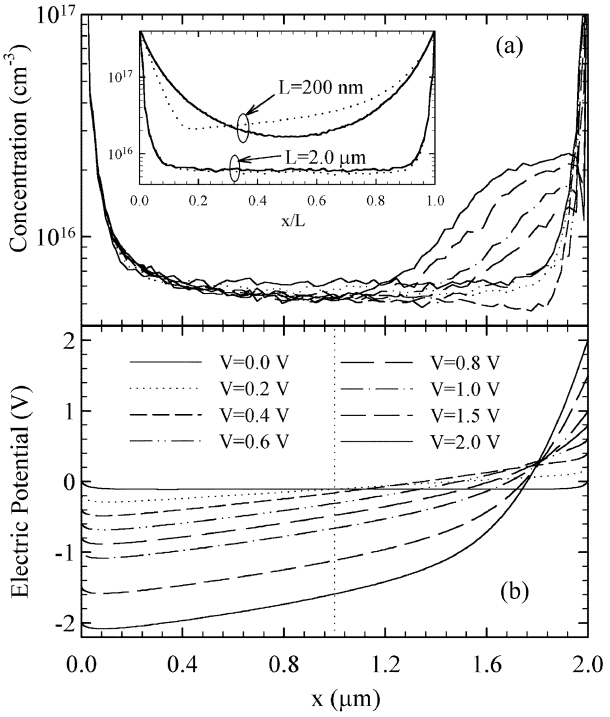

Fig. 4. (a) Profiles of electron concentration. (b) Electric potential along the horizontal branches of the TBJ with $L = 2$ μm for different bias conditions. The inset shows the comparison with the profile of electron concentration in the short TBJ ($L = 200$ nm) for low bias.

region where the slow upper valley electrons are accumulated). Thus, as V increases, the additional potential drop is almost completely restricted to the accumulation region, so that the potential at the midpoint of the TBJ changes following the variations of the negatively biased contact. This effect gives rise also to the saturation of the current–voltage (*I–V*) curves shown in the inset of Fig. 2, and it is quite similar to the traditional mechanism of Gunn effect in the case in which traveling domains cannot be formed, leading to a current limiting behavior (see for example [7]).

This result explains the appearance of negative V_C values in diffusive TBJs, and also the nearly constant unity slope ($|dV_C/dV| \approx 1$) obtained experimentally for $V > 0.2$ V (Fig. 2), both for short and long devices. Indeed, this regime of intervalley transfer is also reached in the short ballistic TBJs, thus making the $V_C(V)$ curve evolve from the low-bias parabolic behavior to the high-bias linear one. Finally, we want to remark that even if the static response is similar in the high-bias diffusive case and in the low-bias ballistic one, the latter provides a much better frequency behavior. This is due to the decrease of the transit time of electrons achieved when the TBJs are downscaled, associated to both the shorter distance to travel and the enhanced ballistic mean velocity (that can be multiplied by 4–5 with respect to the diffusive values).

REFERENCES

[1] A. M. Song, A. Lorke, A. Kriele, J. P. Kothaus, W. Wegscheider, and M. Bichler, "Nonlinear electron transport in an asymmetric microjunction: A ballistic rectifier," *Phys. Rev. Lett.*, vol. 80, pp. 3831–3834, 1998.

[2] A. M. Song, M. Missous, P. Omling, A. R. Peaker, L. Samuelson, and W. Seifert, "Unidirectional electron flow in a nanometer-scale semiconductor channel: A self-switching device," *Appl. Phys. Lett.*, vol. 83, pp. 1881–1883, 2003.

[3] H. Q. Xu, "Electrical properties of three-terminal ballistic junctions," *Appl. Phys. Lett.*, vol. 78, pp. 2064–2066, 2001.

[4] I. Shorubalko, H. Q. Xu, I. Maximov, P. Omling, L. Samuelson, and W. Seifert, "Nonlinear operation of GaInAs–InP-based three-terminal ballistic junctions," *Appl. Phys. Lett.*, vol. 79, pp. 1384–1386, 2001.

[5] J. Mateos, B. G. Vasallo, D. Pardo, T. González, J. S. Galloo, Y. Roelens, S. Bollaert, and A. Cappy, "Ballistic nanodevices for THz data processing: Monte Carlo simulations," *Nanotechnology*, vol. 14, pp. 117–122, 2003.

[6] J. Mateos, B. G. Vasallo, D. Pardo, T. González, J. S. Galloo, S. Bollaert, Y. Roelens, and A. Cappy, "Microscopic modeling of nonlinear transport in ballistic nanodevices," *IEEE Trans. Electron Devices*, vol. 50, pp. 1897–1905, Sept. 2003.

[7] M. Shur, *GaAs Devices and Circuits*. New York: Plenum, 1987.